Lift Coefficients of Clean Ellipsoidal Bubbles in Linear Shear Flows

Hayashi, Kosuke

Legendre, Dominique

Tomiyama, Akio

(Citation)
International Journal of Multiphase Flow,129:103350

(Issue Date)
2020-08

(Resource Type)
journal article

(Version)
Accepted Manuscript

Lift Coefficients of Clean Ellipsoidal Bubbles in Linear Shear Flows

Kosuke Hayashi[a], Dominique Legendre[b], Akio Tomiyama[a,*]

[a] *Graduate School of Engineering, Kobe University, 1-1 Rokkodai Nada Kobe Hyogo, 657-8501 Japan*
[b] *Institut de Mécanique des Fluides de Toulouse (IMFT) - Université de Toulouse, CNRS-INPT-UPS, 2 Allée du Professeur Camille Soula, 31400 Toulouse, France*

Abstract

The lift force acting on an ellipsoidal bubble is known to change its sign, depending on the bubble aspect ratio. The lift reversal has often been modeled in terms of the Eötvös number defined by using the bubble major axis to account for the deformation effect on the negative lift component. This paper presents a physically reliable scaling accounting for the two mechanisms in competition related to the two sources of vorticity: the lift controlled by the shear flow and contribution from the interfacial vorticity source. This scaling is used for developing a correlation that makes possible the lift modeling with the reversal.

Keywords: lift force, lift reversal, negative lift, shape deformation

1. Introduction

Multi-fluid models and bubble tracking methods (Tomiyama, 1998; Lucas et al., 2007; Lucas and Tomiyama, 2011; Hosokawa and Tomiyama, 2009; Darmana et al., 2009) have been widely used to simulate bubbly flows in practical systems. These methods require models of hydrodynamic forces acting on bubbles, e.g. the drag and lift forces. Hence reliable models of these forces are required to obtain accurate predictions. Tomiyama et al. (1998) proposed a drag correlation for a wide range of flow conditions. This correlation has been widely utilized in bubbly flow simulations. The drag coefficient, C_D, in the viscous force dominant regime was developed based on the Hadamard-Rybczynski model (Hadamard, 1911; Rybczynski, 1911) extended by accounting for an inertial effect and Levich's drag model. The aspect

*Corresponding author
Email address: tomiyama@mech.kobe-u.ac.jp (Akio Tomiyama)

ratio of a bubble however does not appear in this correlation. Rastello et al. (2011) extended Mei's drag correlation for clean spherical bubbles (Mei et al., 1994) to account for the effects of the bubble aspect ratio. The Rastello correlation has been confirmed to be more accurate than other available drag correlations for the viscous force dominant regime. Its functional form is however somewhat complicated. Chen et al. (2019) therefore proposed a simpler drag correlation accounting for the aspect ratio effect by extending the Tomiyama correlation, and the correlation makes use of the aspect ratio correlation proposed by Aoyama et al. (2016). Drag coefficients of clean ellipsoidal bubbles in the surface tension force dominant regime can be accurately evaluated using another Tomiyama's correlation (Tomiyama et al., 2002) expressed in terms of the Eötvös number. Ziegenhein et al. (2018) confirmed that the drag correlation proposed by Bozzano and Dente (2001) also agrees with their experimental data in the surface tension force dominant regime. The drag coefficients of clean ellipsoidal bubbles can thus be accurately evaluated by using the available correlations. On the other hand, the accuracy of available lift coefficient correlations is still insufficient.

A shear-induced lift force acting on a bubble is usually expressed as (Žun, 1980; Auton, 1987; Auton et al., 1988; Legendre and Magnaudet, 1998)

$$\boldsymbol{F}_L = -C_L(\rho_L \pi d^3/6)\boldsymbol{V}_R \times \nabla \times \boldsymbol{V}_L \tag{1}$$

where C_L is the lift coefficient, ρ_L the liquid density, d the sphere-volume-equivalent bubble diameter, and $\boldsymbol{V}_R$ the bubble velocity relative to the liquid velocity $\boldsymbol{V}_L$. Auton (1987) derived an analytical solution, $C_L^{S\infty}$, of C_L for a spherical bubble in a linear shear flow of an inviscid fluid:

$$C_L^{S\infty} = 1/2 \tag{2}$$

where the superscript S denotes a spherical bubble. Legendre and Magnaudet (1998) carried out numerical simulations of spherical bubbles in linear shear flows. Their numerical results showed that C_L^S approaches $C_L^{S\infty}$ as the bubble Reynolds number, Re, increases and they obtained the following empirical correlation for bubbles of intermediate and high Reynolds numbers:

$$C_L^{SH} = \frac{1}{2}\left(\frac{1+16/Re}{1+29/Re}\right) \tag{3}$$

where the superscript H denotes high Reynolds numbers and

$$Re = \rho_L V_R d/\mu_L \tag{4}$$

where μ_L is the liquid viscosity and $V_R = |\boldsymbol{V}_R|$. Legendre and Magnaudet (1997, 1998) applied a matched asymptotic procedure to a low Re bubble and derived the following C_L in the Stokes regime:

$$C_L^{SL} = \frac{6}{\pi^2}\frac{2.255}{\sqrt{SrRe}\,[1+0.2Re/Sr]^{3/2}} \tag{5}$$

where the superscript L denotes low Reynolds numbers ($Re < 1$) and Sr is the dimensionless shear rate defined by

$$Sr = \Omega d/V_R \tag{6}$$

and Ω is the shear rate (vorticity) of a linear shear flow. Legendre and Magnaudet (1998) combined Eqs. (3) and (5) to cover a wide range of Re as follows:

$$C_L^S = ([C_L^{SL}]^2 + [C_L^{SH}]^2)^{1/2} \tag{7}$$

This correlation was confirmed to give good evaluations of C_L for spherical bubbles for a wide range of Re (Aoyama et al., 2017).

A deformed bubble is known to have a negative lift coefficient and laterally migrates in the direction opposite to a spherical bubble. Kariyasaki (1987) found in his experimental study on the motion of bubbles in linear shear flows that the direction of the lift force acting on a deformed bubble is opposite to that on a solid sphere. The reversal of the lift force was also observed in numerical simulations of two-dimensional bubbles (Tomiyama et al., 1993), in experiments of ellipsoidal bubbles (Tomiyama, 1998; Tomiyama et al., 2002; Tomiyama, 2004) and in three-dimensional single bubble simulations (Ervin and Tryggvason, 1997; Bothe et al., 2006; Adoua et al., 2009; Dijkhuizen et al., 2010; Hayashi and Tomiyama, 2018). The above-mentioned C_L models for spherical bubbles give positive values at any Re, and therefore, the negative component of the lift force has been considered to have a relation with the shape deformation of a bubble. Adoua et al. (2009) carried out numerical simulations of ellipsoidal bubbles of various aspect ratios to investigate the mechanism of

the reversal of the lift force. They pointed out that the interaction between the vorticity, Ω, of the uniform shear and the vorticity, ω, generated at the bubble surface plays a key role in the lift reversal. Tomiyama et al. (2002) took into account the deformation effect by using the major axis, d_H, of a bubble as the characteristic length scale to correlate C_L:

$$C_L = \begin{cases} \min[0.288\tanh(0.121Re), f_T(Eo_H)] & \text{for } Eo_H < 4 \\ f_T(Eo_H) & \text{for } 4 \le Eo_H \le 10.7 \end{cases} \tag{8}$$

where

$$f_T(Eo_H) = 0.00105Eo_H^3 - 0.0159E_H^2 - 0.0204Eo_H + 0.474 \tag{9}$$

and Eo_H is the Eötvös number defined by

$$Eo_H = \Delta\rho g d_H^2/\sigma \tag{10}$$

Here $\Delta\rho$ is the difference between the liquid and gas densities, g the magnitude of the acceleration of gravity and σ the surface tension. The function of Re ($C_L = 0.288\tanh(0.121Re)$) is for small bubbles of positive lift, whereas $f_T(Eo_H)$ is used for deformed bubbles of positive or negative lift. Dijkhuizen et al. (2010) carried out numerical simulations of single bubbles in linear shear flows and correlated C_L in the following form:

$$C_L = \min\left[C_L^S, f_D(Eo_H)\right] \tag{11}$$

$$f_D(Eo_H) = 0.5 - 0.11Eo_H + 0.002Eo_H^2 \tag{12}$$

where C_L^S is given by Eq. (7). Ziegenhein et al. (2018) and Lucas and Ziegenhein (2019) proposed the following empirical correlation for $Eo_H > 1.2$:

$$C_L = \max\left[f_Z(Eo_H), -0.33\right] \tag{13}$$

$$f_Z(Eo_H) = 0.5 - 0.1Eo_H + 0.002Eo_H^2 \tag{14}$$

where the second coefficient of f_Z was slightly modified from that of f_D by fitting the functional form to Ziegenhein's data for bubbles in a low viscosity system. Figure 1 compares C_L data (Aoyama et al., 2017) with the correlations, f_T, f_D and f_Z, for deformed bubbles. As Aoyama et al. (2017) pointed out, the data for various Morton numbers, M, cannot be

correlated only with Eo_H, and the functions of Eo_H for the Eo-regime cannot account for the Morton number dependence, where M is defined by

$$M = \frac{\mu_L^4 \Delta\rho g}{\rho_L^2 \sigma^3} \tag{15}$$

Though an accurate evaluation of the lift force is indispensable in multi-fluid and bubble tracking simulations to obtain good predictions, the available C_L correlations do not satisfactorily account for the characteristics of C_L of ellipsoidal bubbles. In this study we consider physical arguments for scaling of C_L of single clean ellipsoidal bubbles by making use of the experimental data of C_L (Aoyama et al., 2017) to obtain the basis for development of a C_L correlation applicable to a wide range of relevant dimensionless parameters and to reproduce the lift reversal induced by deformation.

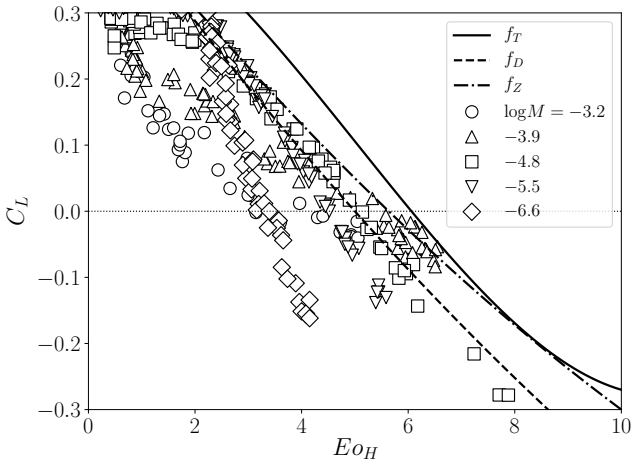

Figure 1: C_L plotted against Eo_H and comparison with available correlations (data quoted from Aoyama et al. (2017))

2. Dataset

Aoyama et al. (2017) carried out experiments on single air bubbles in liner shear flows to obtain a C_L database. The measured C_L, C_D, Re, Sr and bubble aspect ratios, χ $(= d_H/d_V)$, were tabulated in their paper, where d_V is the minor axis of an ellipsoidal bubble. It should be noted that the aspect ratio, E, in Aoyama et al. (2017) is the inverse of the present

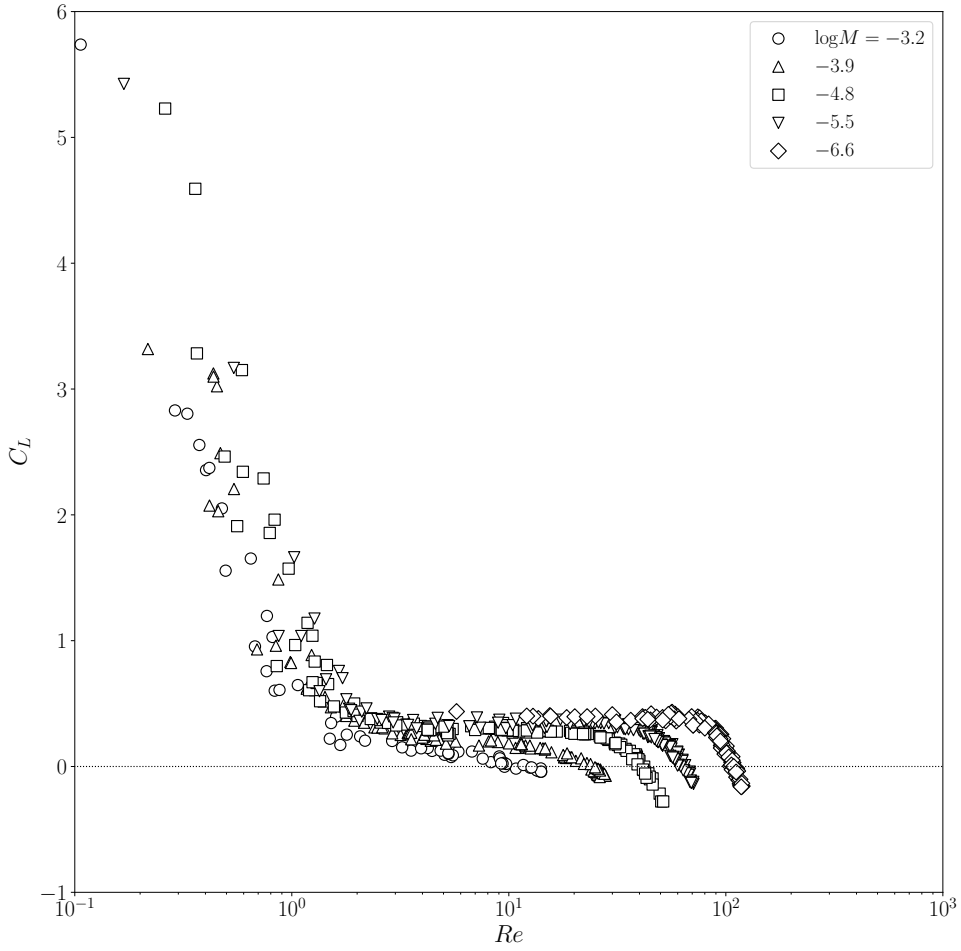

Figure 2: Dataset of C_L quoted from Aoyama et al. (2017) ($-6.6 \leq \log M \leq -3.2$)

definition, i.e. $E = 1/\chi$. Liquid flows in their experiments were laminar and no turbulent effects were present in the transverse motion of bubbles.

Figure 2 shows the dataset of C_L. The range of M is $-6.6 \leq \log M \leq -3.2$. The Aoyama data cover low to intermediate Re, i.e. $0.1 < Re < 120$, in which the bubble shape changes from sphere to ellipsoid with increasing Re. The C_L for $Re < 1$ decreases as Re increases. The rate of decrease in C_L becomes smaller for $Re > 1$, while C_L decreases and falls into the negative lift regime at a certain Re depending on M. The ranges of the relevant dimensionless groups in the dataset are shown in Table 1. The C_D in the dataset are also shown in Fig. 3.

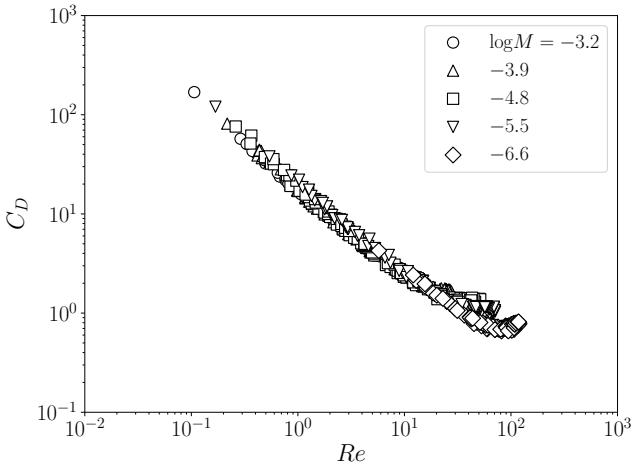

Figure 3: Dataset of C_D quoted from Aoyama et al. (2017) ($-6.6 \leq \log M \leq -3.2$)

Table 1: Ranges of dimensionless groups in dataset

log$M$	-3.2	-3.9	-4.8	-5.5	-6.6
Number of data	56	114	139	146	107
Re	0.11-14	0.22-28	0.26-51	0.17-71	5.7-120
Eo	0.11-4.2	0.10-5.0	0.063-5.0	0.027-3.7	0.14-2.6
Sr	0.088-0.43	0.076-0.42	0.059-0.34	0.048-0.26	0.034-0.077
χ	1.0-1.35	1.0-1.6	1.0-2.0	1.0-1.96	1.0-2.0
C_D	2.3-169	1.6-81	1.2-76	0.93-121	0.66-4.3
C_L	-0.042-5.7	-0.084-3.3	-0.28-5.22	-0.14-5.4	-0.16-0.44

Figure 4 shows a *Re*-*Eo* map (Tomiyama et al., 1998) and the dataset are plotted on it, where Eo is the Eötvös number defined by

$$Eo = \Delta\rho g d^2/\sigma \tag{16}$$

The dashed line represents the transition boundary between the Re-controlling regime ($C_D = H/Re$ where $H = 48$ (Levich, 1962) or $16(1 + 0.15Re^{0.687})$ (Schiller and Nauman, 1933)) and the Eo-controlling regime ($C_D = 8Eo/3(Eo + 4)$). Most of the data lie below the transition boundary and Aoyama et al. (2017) confirmed that bubbles rose rectilinearly with no path/shape oscillation, and therefore, they were in the viscous force dominant regime.

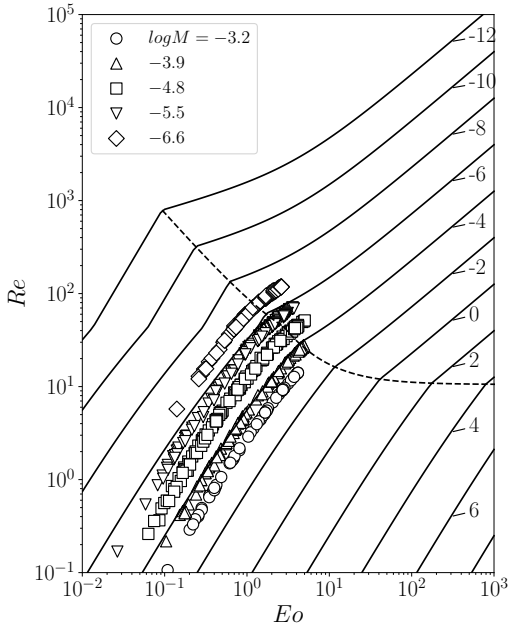

Figure 4: Dataset on *Re-Eo* plane (Tomiyama et al., 1998). Labels represent log$M$

3. Scaling for Lift Reversal

3.1. Effects of Deformation and Reynolds Number on Negative Lift

Naciri (1992) showed that C_L of a bubble of non-deformable ellipsoidal shape in a weak inviscid shear flow increases with increasing the shape deformation. Numerical simulations of ellipsoidal bubbles carried out by Adoua et al. (2009) reproduced Naciri's results, and they obtained the following empirical correlation:

$$C_L = 0.5 g_N(\chi) \tag{17}$$

where g_N is the deformation effect multiplier given by

$$g_N = 1 + 1.22(\chi - 1) \tag{18}$$

This correlation can be regarded as an extension of Auton's solution for a spherical bubble at high Re, i.e. $C_L^{S\infty} = 1/2$. The χ increases with increasing Re, and therefore, according to Eq. (17) C_L increases with Re. This tendency does not agree with the experimental results as shown in Fig. 5, and therefore, the Naciri solution does not serve as a base for

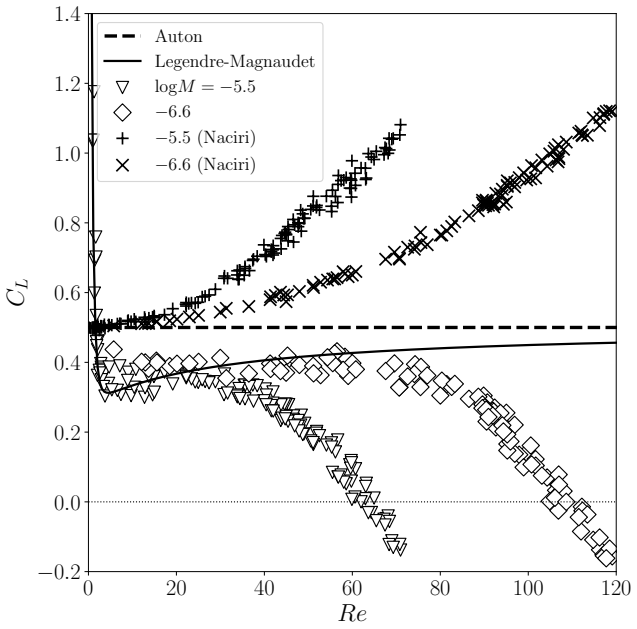

Figure 5: C_L data of $\log M = -5.5$ and -6.6 compared with available C_L correlations, i.e. Eqs. (2), (7) and (17)

the description of the lift for large Re. The deviation of Eq. (17) from the data may be due to the shape effect, i.e., the bubble shape is not an exact ellipsoid and shows fore-aft and left-right asymmetries in reality, which was not accounted for in their simulation in spite of the strong sensitivity of the lift to shape deformation. The dependence of C_L on Re observed in the experiments was reproduced in level set simulations (Hayashi and Tomiyama, 2018), in which the deviation of the bubble shape from the exact ellipsoid was accounted for. This fact supports the above speculation.

As Re increases, Eq. (3) asymptotically approaches

$$C_L^S = 0.5 - \frac{6.5}{Re} \tag{19}$$

The viscous contribution to the lift force behaves like Re^{-1} and it coincides with the well-known behavior of the drag force, i.e. $C_D = 48/Re$ (Levich, 1962). This drag force results from the existence of a thin layer of vorticity on the bubble surface of magnitude $\omega = \mathrm{O}(U/r)$, where $r = d/2$ (Legendre, 2007). When a bubble deforms while keeping an ellipsoidal shape, the vorticity generated at the bubble surface is known to increase with the shape deformation

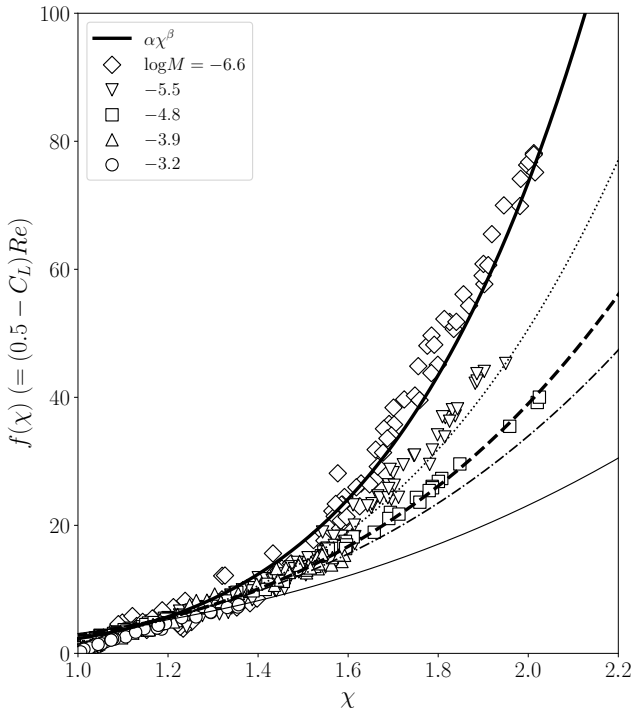

Figure 6: Deformation effect multiplier, $f(\chi)$ $(= (1/2 - C_L)Re)$. The lines represent $f(\chi) = \alpha\chi^\beta$ (see Table 2 for the values of α and β).

as $\omega = \mathrm{O}(\chi^3 U/r_H)$, where $r_H = d_H/2$ (Adoua et al., 2009; Magnaudet and Mougin, 2007). As a consequence a similar effect on the bubble lift can be speculated as

$$C_L = 0.5 - \frac{f(\chi)}{Re} \tag{20}$$

where $f(\chi)$ is a function accounting for the negative lift component due to shape deformation. As explained in Adoua et al. (2009) the tilt and stretching of the interfacial vorticity results in the generation of a downstream axial vorticity in the opposite direction of rotation, which is generated by the incident vorticity of the shear flow. This results in a reversal of the lift. Let us check the validity of the speculation for the C_L data by using Eq. (20). Figure 6 shows $f(\chi) = (0.5 - C_L)Re$, which clearly shows that the deformation effect on C_L is well scaled with the factor of Re^{-1} and χ is a primal factor correlating the deformation effect. The lines are the following fitting equation: $f(\chi) = \alpha\chi^\beta$, where the coefficients, α and β, are adjusted for each Morton number system as given in Table 2. Equation (20) can therefore

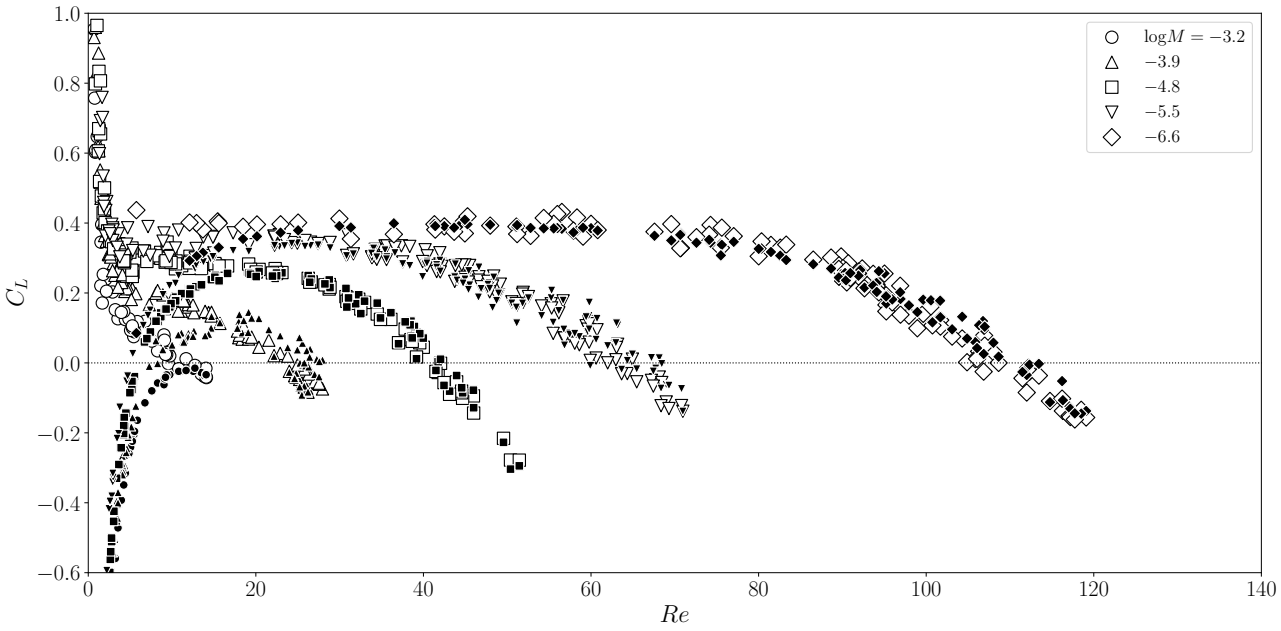

Figure 7: Eq. (21) with coefficients in Table 2. Closed symbols: calculated values, Open symbols: experimental data.

be rewritten as

$$C_L = 0.5 - \frac{\alpha \chi^{\beta}}{Re} \tag{21}$$

Comparisons between Eq. (21) and the C_L data are shown in Fig. 7. Equation (21) is able to reproduce the C_L decrease and the lift reversal. However Eq. (21) cannot be applied to low Re. Indeed, when $Re \to 0$ the trend in Re^{-1} dominates and imposes a decay of the lift.

Table 2: Coefficients in Eq. (21)

log$M$	−3.2	−3.9	−4.8	−5.5	−6.6
α	3.1	3.0	2.8	2.4	2.3
β	2.9	3.5	3.8	4.4	5

3.2. Physical Description of Lift Reversal

The simple analysis in the previous section clearly showed that (1) the functional form of the viscous contribution in the negative lift is similar to the drag, i.e. Re^{-1}, and (2) the shape

deformation increases the negative lift. In fact, the relation, Eq. (21), would be justified as the consequence of two conjugate effects: the drag is proportional to the interfacial vorticity (Legendre, 2007) and the lift reversal is induced by the interfacial vorticity (Adoua et al., 2009)). Therefore the reversal in the lift of ellipsoidal bubbles can be connected to the drag:

$$C_L = 0.5 - G(\chi, Re) C_D \tag{22}$$

where $G(\chi, Re)$ is a function of χ and Re.

Let us discuss the contributions of χ and Re to the lift reversal by investigating the functional form of C_D in terms of χ and Re. Legendre (2007) pointed out that C_D of ellipsoidal bubbles is expressed as

$$C_D = \frac{16}{Re} f_d(\chi, Re) \omega^*_{\max}(\chi, Re) \tag{23}$$

where $\omega^*_{\max}$ $(= \omega_{\max} r/U)$ is the dimensionless maximum vorticity produced at the bubble surface and $f_d(\chi, Re)$ the deformation effect multiplier. Although numerical results of f_d and $\omega_{\max}$ were graphically given in Legendre (2007), their functional forms have not been obtained. In the following, we therefore make use of the vorticity in the infinite Reynolds number limit (Magnaudet and Mougin, 2007) and the deformation multiplier (Legendre, 2007) obtained by using Moore's drag model for high Reynolds number bubbles (Moore, 1965) to express the drag as $C_D(\chi, Re)$. Magnaudet and Mougin (2007) derived $\omega^*_{\max}$ as a function only of χ in the infinite Re limit, i.e.

$$\omega^{*\infty}_{\max}(\chi) = \frac{2\chi^{5/3}(\chi^2-1)^{3/2}}{\chi^2 \sec^{-1}\chi - (\chi^2-1)^{1/2}} \tag{24}$$

where $\omega^{*\infty}_{\max} \to 4\chi^{8/3}/\pi$ as χ becomes very large, i.e. $\sec^{-1}\chi \to \pi/2$. Moore (1965) derived the following C_D model of ellipsoidal bubbles at high Re:

$$C_D = \frac{16}{Re} \frac{\chi^{4/3}(\chi^2-1)^{3/2}\left[(\chi^2-1)^{1/2} - (2-\chi^2)\sec^{-1}\chi\right]}{\left[\chi^2 \sec^{-1}\chi - (\chi^2-1)^{1/2}\right]^2} \tag{25}$$

By combining this model and Eq. (24), $f_d^\infty(\chi)$ $(= f_d(\chi, \infty))$ can be expressed as (Legendre, 2007)

$$f_d^\infty(\chi) = \frac{1}{2\chi^{1/3}} \frac{(\chi^2-1)^{1/2} - (2-\chi^2)\sec^{-1}\chi}{\chi^2 \sec^{-1}\chi - (\chi^2-1)^{1/2}} \tag{26}$$

Equation (23) can therefore be written as

$$C_D = \frac{16}{Re} F(\chi, Re) f_d^{\infty} \omega_{\max}^{*\infty} \tag{27}$$

where $F(\chi, Re)$ is a multiplier connecting C_D with that at high Re, i.e. $C_D^H(\chi, Re) = 16 f_d^{\infty} \omega_{\max}^{*\infty}/Re$ (Moore drag). The $F(\chi, Re)$ calculated using the present dataset is shown in Fig. 8. It increases with increasing χ and approaches a constant value depending on M. Chen et al. (2019) proposed the following empirical drag correlation for ellipsoidal bubbles in the viscous force dominant regime:

$$C_D = \frac{16}{Re} \left[1 + \phi(\chi, Re)\right] \tag{28}$$

where the second term in the brackets is a function for the deformation-inertia effect multiplier:

$$\phi(\chi, Re) = 0.25 \chi^{1.9} Re^{0.32} \tag{29}$$

The M dependence of $F(\chi, Re)$ is well expressed using ϕ as shown in Fig. 9. The ratio, $F(\chi, Re)/\phi(\chi, Re)$, of deformed bubbles is a function of χ, and $F(\chi, Re)$ can be fitted as $F(\chi, Re) = 0.91 f_d^{\infty}(\chi)^{3.65} \phi(\chi, Re)$. Hence

$$C_D(\chi, Re) = \frac{16}{Re} (0.91 f_d^{\infty}(\chi)^{4.65}) \phi(\chi, Re) \omega_{\max}^{*\infty}(\chi) \tag{30}$$

It should be noted that this expression is valid for deformed bubbles of χ larger than about 1.1.

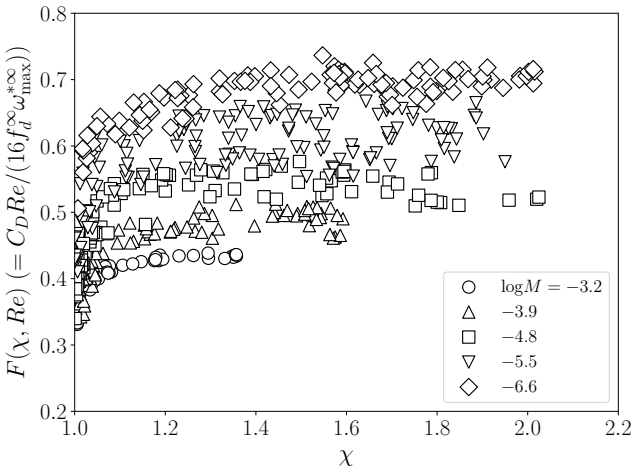

Figure 8: Function, $F(\chi, Re) = C_D Re/(16 f_d^{\infty} \omega_{\max}^{*\infty})$, connecting C_D with that at high Re

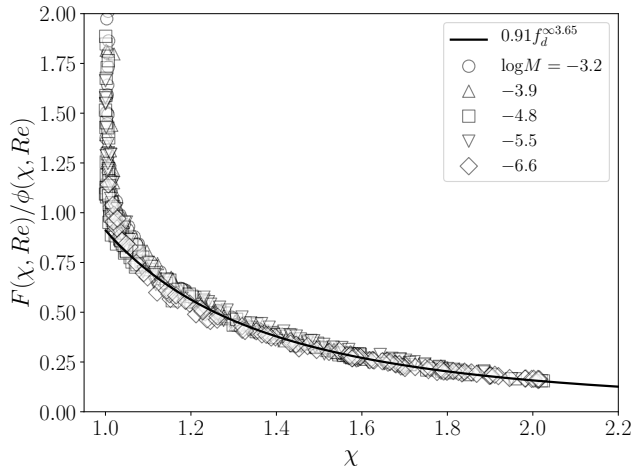

Figure 9: $F(\chi, Re)/\phi(\chi, Re)$

Then let us consider the functional form of G in Eq. (22). The G calculated from the database is shown in Fig. 10, in which f_d^{∞} is used for the horizontal axis. The collapse of the data onto the single curve expressed as $0.086/f_d^{\infty 4.65}$ means that G is a function of χ and the product GC_D can be approximated as $GC_D \sim 16\gamma\phi\omega_{\max}^{*\infty}/Re$, where $\gamma = 0.078$. Substituting this approximation into Eq. (22) yields

$$C_L = 0.5 - \gamma \frac{16}{Re} \phi(\chi, Re) \omega_{\max}^{*\infty}(\chi) \tag{31}$$

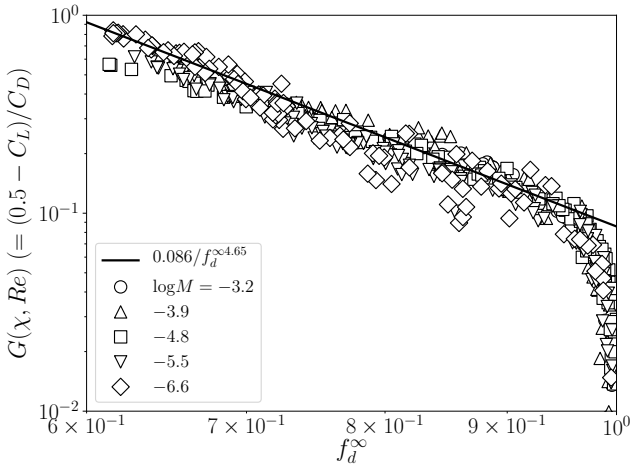

Figure 10: $G(\chi, Re)$ in Eq. (22)

Expanding this equation using Eqs. (24) and (29) gives

$$C_L = 0.5 - \gamma \frac{4\chi^{1.9} Re^{0.32}}{Re} \left[\frac{2\chi^{5/3}(\chi^2 - 1)^{3/2}}{\chi^2 \sec^{-1}\chi - (\chi^2 - 1)^{1/2}} \right] \tag{32}$$

This equation well expresses the decay of C_L due to the increase in the negative lift as Re increases as shown in Fig. 11. Thus it has become clearer that the negative lift is correlated with the drag, and in both forces ω plays an important role. It is interesting that the part of C_D, i.e. $f_d^{\infty 4.65}$, relating with the correction factor f_d^∞ does not appear in the negative lift.

4. Lift Coefficient Correlation

The lift reversal has been well scaled in terms of Re and χ. Then we have to find an appropriate expression for the lift coefficient for spherical and ellipsoidal bubbles with a good compromise between physical consistency and fitting efficiency. The functional form of Eq. (21) needs to be connected with C_L at small Reynolds number.

As shown in Fig. 5, C_L of ellipsoidal bubbles are smaller than $C_L^{S\infty} = 0.5$. However they agree with the Legendre-Magnaudet correlation up to certain Re, e.g. $Re < 60$ at $\log M = -6.6$ and $Re < 20$ at $\log M = -5.5$. We therefore use C_L^S given by Eq. (7) as the

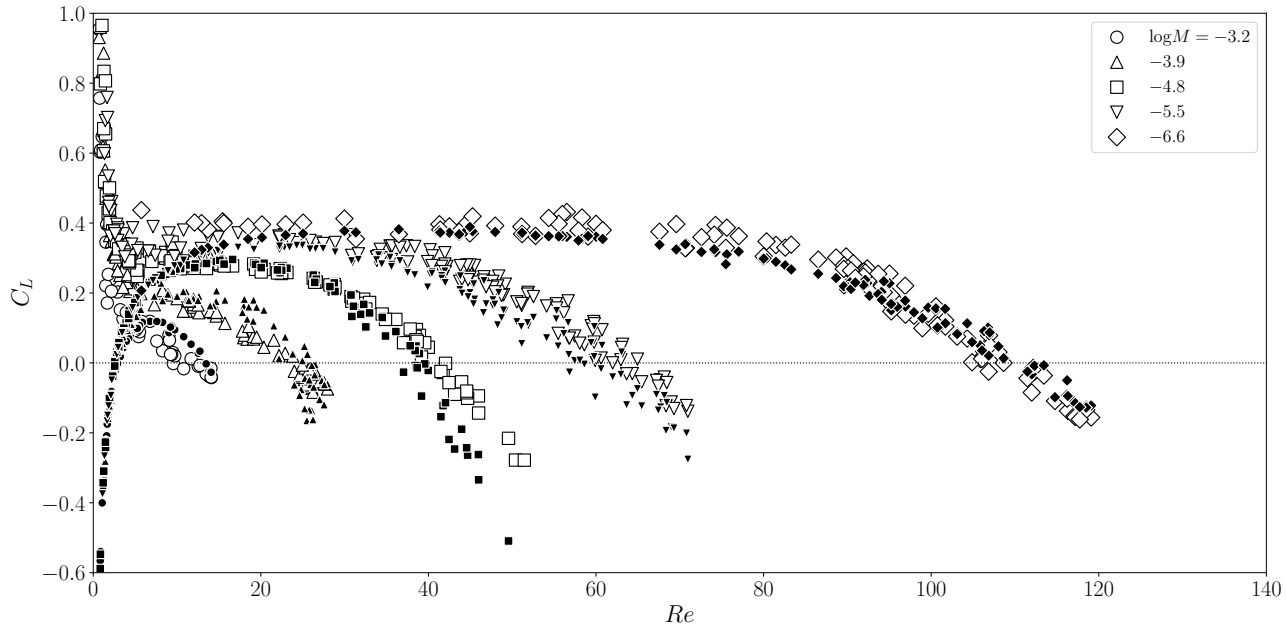

Figure 11: Equation (32) compared with measured data. Closed symbols: calculated values, Open symbols: experimental data.

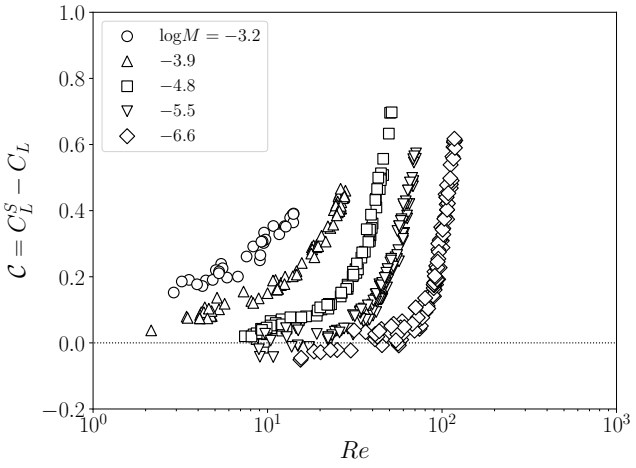

Figure 12: $\mathcal{C} = C_L^S - C_L$ ($\chi > 1.02$)

basis of an expression for ellipsoidal bubbles instead of $C_L^{S\infty}$ ($= 0.5$):

$$C_L = C_L^S - \mathcal{C} \tag{33}$$

where $\mathcal{C}$ is the component for the negative lift due to shape deformation. Figure 12 shows

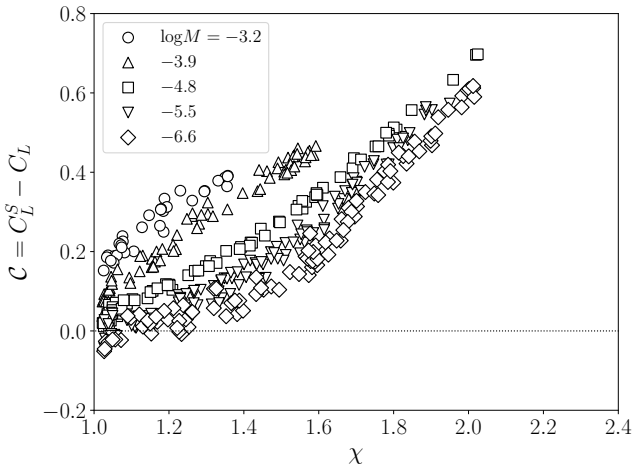

Figure 13: $\mathcal{C}$ plotted against χ ($\chi > 1.02$)

$\mathcal{C} = C_L^S - C_L$, where only data of $\chi > 1.02$ (deformed bubbles) are used. The negative lift component clearly increases with increasing Re. It would be better to use a dimensionless group more tightly relating with shape deformation, e.g. Eo_H (Tomiyama et al., 2002) or $Eo^{1.1}Re$ (Aoyama et al., 2017), or a shape parameter, i.e. χ, instead of Re. The function $\mathcal{C}$ is therefore replotted against χ in Fig. 13. The fact that the negative lift is produced by the shape deformation effect can be more clearly observed, i.e. $\mathcal{C}$ increases with increasing χ. The magnitude of $\mathcal{C}$ depends on M, e.g. even at the same χ ($\chi \approx 1.02$), i.e. $\mathcal{C} \approx 0.2$ at log$M = -3.2$ whereas $\mathcal{C} \approx 0$ at log$M = -6.6$.

As already confirmed in Fig. 7, the negative lift can be correlated in terms of χ and Re at each M. The Morton number is therefore used as an additional parameter in correlating $\mathcal{C}$ due to the following reasons: M consists of the three representative dimensionless groups, i.e. $M = EoCa^2/Re^2$, where Ca ($= \mu_L V_R/\sigma$) is the Capillary number representing the ratio of the viscous force to the surface tension force. Owing to its structure, M can be used to represent complex behavior of C_L. Furthermore, as reported by Tsuge and Hibino (1977), the critical Reynolds number, Re_O, for the instability of the wake behind a bubble causing bubble oscillatory motion is given by $Re_O = 9M^{-0.173}$, the trend of which is the same as the critical Reynolds number for the reversal of the sign of C_L for $-6.6 \leq \log M \leq -3.2$ (Aoyama et al., 2017). This is due to the fact that the wake instability plays a key role in

Table 3: Coefficients in Eq. (34)

$\log M$	-3.2	-3.9	-4.8	-5.5	-6.6
g	14.8	24.2	33.6	49.3	71.7
h	0.98	1.23	1.73	2.30	2.53

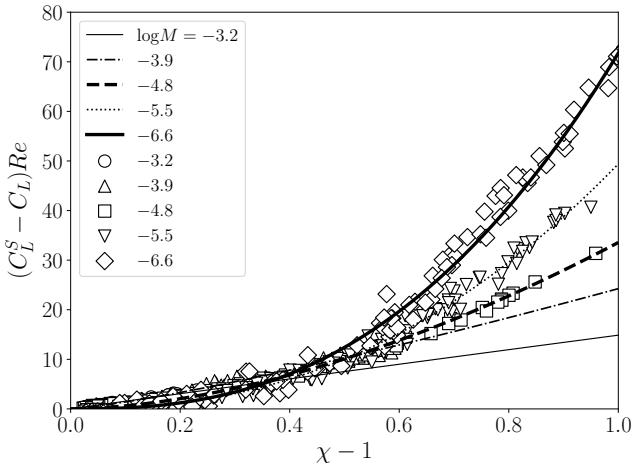

Figure 14: $(C_L^S - C_L)Re$ ($\chi > 1.02$). Curves are fitted to data in terms of $g(\chi - 1)^h$.

the lift reversal as pointed out by Adoua et al. (2009). Hence we assume the following form for C_L:

$$C_L = C_L^S - \frac{g(M)(\chi - 1)^{h(M)}}{Re} \tag{34}$$

It should be noted that χ in Eq. (21) was replaced with $\chi - 1$ in this expression to make $C_L \to C_L^S$ as $\chi \to 1$, and the coefficients, g and h, in the second term should be expressed in terms of M to account for the M effect on the negative lift. The $\mathcal{C}$ scaled with Re^{-1} is shown in Fig. 14, where g and h are obtained by fitting to the data as shown in Table 3. Figure 15 shows comparisons between the data and Eq. (34). Good agreements are obtained although errors tend to be large in the transition from spherical to ellipsoidal shapes as seen in $\log M = -4.8$, i.e. $5 < Re < 20$ ($1.02 < \chi < 1.18$).

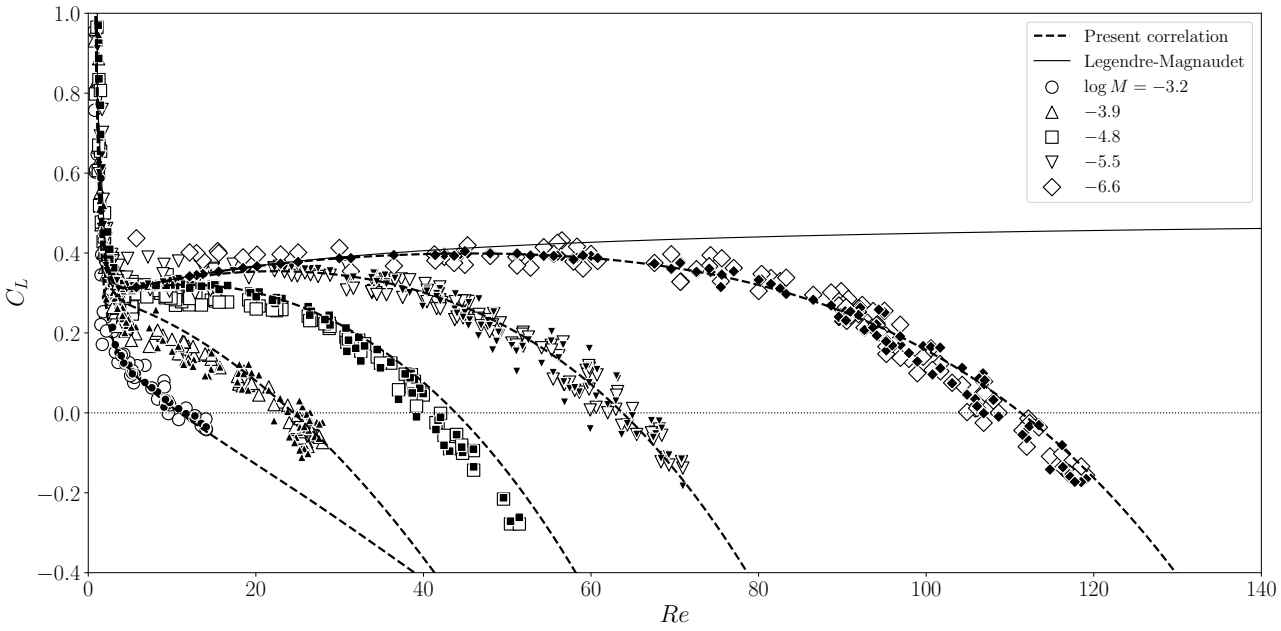

Figure 15: Comparison of empirical correlation, Eq. (34), with C_L dataset. Closed symbols: calculated with Eq. (34), Open symbols: experimental data. C_L curves (dashed lines) are also drawn using Eq. (34) with the Aoyama and Chen correlations to evaluate χ and Re. The lines are drawn with $Sr = 0.1$.

The coefficients are given by

$$g(M) = a\exp(-bM^c) \tag{35}$$

$$h(M) = p\exp(-qM^r) \tag{36}$$

where $a = 500, b = 6.0, c = 0.0735, p = 3.46, q = 5.4$ and $r = 0.191$.

To evaluate C_L of clean ellipsoidal bubbles using Eq. (34), a correlation of χ is required. Aoyama et al. (2016) proposed the following χ correlation for clean ellipsoidal bubbles in
225 the viscous force dominant regime:

$$\chi = (1 + 0.016Eo^{1.12}Re)^{0.388} \tag{37}$$

Substituting this correlation into the Chen correlation (Chen et al., 2019), Eq. (28), gives good evaluations of Re. Equations (28) and (37) were therefore used to evaluate Re and χ. The broken lines in Fig. 15 are drawn by using Eq. (28), (34) and (37), which agrees well with the experimental data. Figure 16 shows Eq. (34) drawn against Eo_H. Equation (34)

expresses well the complex trend of C_L against Eo_H. The predictions taking into account the effects of M are better than the available correlations for ellipsoidal bubbles shown in Fig. 1.

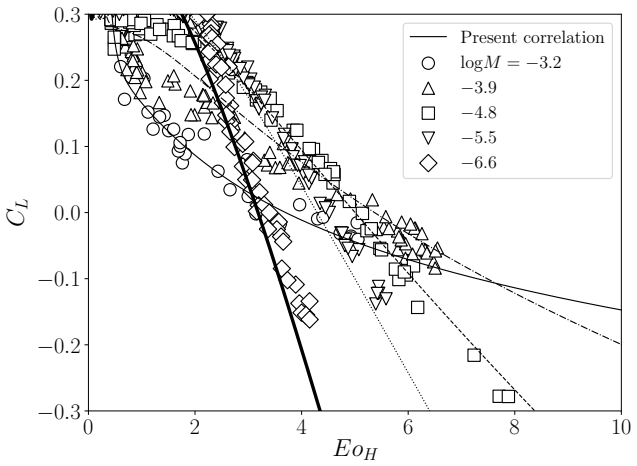

Figure 16: C_L curves drawn for Eo_H by using Eq. (34) (Legends are the same as in Fig. 14)

5. Conclusion

Scaling for the lift force acting on single ellipsoidal bubbles in linear shear flows was carried out. The Naciri solution, Eq. (17), for ellipsoidal bubbles does not serve as a base for the description of the lift for large Re observed in the experiments by Aoyama et al. (2017), i.e. the lift coefficient, C_L, increases with Re in the Naciri solution, while the measured C_L of ellipsoidal bubbles decreases with increasing Re. To reproduce the correct tendency of C_L we proposed a simple scaling, Eq. (21), which clearly includes the two mechanisms in competition related to the two sources of vorticity: the lift controlled by the shear flow ($C_L = 0.5$), i.e. the positive component, and contribution from the interface vorticity source ($C_L \sim -\chi^\beta Re^{-1}$), the negative component. The negative lift was found to be clearly related with the drag, and in both forces the vorticity produced at the bubble surface plays a key role. The scaling was then used to develop a lift correlation, in which the negative lift scaled with $\alpha\chi^\beta/Re$ is connected to the lift coefficient, C_L^S, of spherical bubbles deduced by Legendre and Magnaudet (1998), i.e. $C_L = C_L^S - g(M)(\chi - 1)^{h(M)}/Re$.

This correlation agrees well with the experimental data for $-6.6 \leq \log M \leq -3.2$ and the complex behavior of C_L on the Eo_H-C_L plane is well reproduced. Bubbles in this study are in the viscous force dominant regime, while those at a larger Reynolds number or a lower Morton number could be in the surface tension-inertial force dominant regime. It should be examined whether the present scaling for C_L is applicable to the latter case or not. We will report some results of an application of the scaling to bubbles in the surface tension-inertial force dominant regime in the near future.

Acknowledgement

A. Tomiyama and K. Hayashi would like to express their thanks to financial supports by JSPS KAKENHI, Grant No. 18H03756 and 17K06158.

References

Adoua, R., Legendre, D., Magnaudet, J., 2009. Reversal of the lift force on an oblate bubble in a weakly viscous linear shear flow. Journal of Fluid Mechanics 628, 23–41.

Aoyama, S., Hayashi, K., Hosokawa, S., Lucas, D., Tomiyama, A., 2017. Lift force acting on single bubbles in linear shear flows. International Journal of Multiphase Flow 96, 113–122.

Aoyama, S., Hayashi, K., Hosokawa, S., Tomiyama, A., 2016. Shapes of ellipsoidal bubbles in infinite stagnant liquids. International Journal of Multiphase Flow 79, 23–30.

Auton, T. R., 1987. The lift force on a spherical body in a rotational flow. Journal of Fluid Mechanics 183, 199–218.

Auton, T. R., Hunt, J. C. R., Prud'homme, M., 1988. The force exerted on a body in inviscid unsteady non-uniform rotational flow. Journal of Fluid Mechanics 197, 241–257.

Bothe, D., Schmidtke, M., Warnecke, H.-J., 2006. VOF-simulation of the lift force for single bubbles in a simple shear flow. Chemical Engineering Technology 29, 1048–1053.

Bozzano, G., Dente, M., 2001. Shape and terminal velocity of single bubble motion: a novel approach. Computers and Chemical Engineering 25, 571–576.

Chen, J., Hayashi, K., Hosokawa, S., Tomiyama, A., 2019. Drag correlations of ellipsoidal bubbles in clean and fully-contaminated systems. Multiphase Science and Technology 31(3), 215–234.

Darmana, D., Deen, N. G., Kuipers, J. A. M., Harteveld, W. K., Mudde, R. F., 2009. Numerical study of homogeneous bubbly flow: influence of the inlet conditions to the hydrodynamic behavior. International Journal of Multiphase Flow 35, 1077–1099.

Dijkhuizen, W., van Sint Annaland, M., Kuipers, J. A. M., 2010. Numerical and experimental investigation of lift force on single bubbles. Chemical Engineering Science 65, 1274–1287.

Ervin, E., Tryggvason, G., 1997. The rise of bubbles in a vertical shear flow. Journal of Fluids Engineering 119, 443–448.

Hadamard, J. S., 1911. Mouvement permanent tent d'une sphere liquide et visquese dans un liquide visqueux. Comptes Rendus de l'Academie des Science 152, 1735–1738.

Hayashi, K., Tomiyama, A., 2018. Effects of surfactant on lift coefficients of bubbles in linear shear flows. International Journal of Multiphase Flow 99, 86–93.

Hosokawa, S., Tomiyama, A., 2009. Multi-fluid simulation of turbulent bubbly pipe flows. Chemical Engineering Science 64, 5308–5318.

Kariyasaki, A., 1987. Behavior of a gas bubble in a liquid velocity profile. Transactions of Japan Society of Mechanical Engineers, Series B (in Japanese) 53, 744–749.

Legendre, D., 2007. On the relation between the drag and the vorticity produced on a clean bubble. Physics of Fluids 19, 018102.

Legendre, D., Magnaudet, J., 1997. A note on the lift force on a spherical bubble or drop in a low-Reynolds-number shear flow. Physics of Fluids 9, 3572–3574.

Legendre, D., Magnaudet, J., 1998. The lift force on a spherical bubble in a viscous linear shear flow. Journal of Fluid Mechanics 368, 81–126.

Levich, V., 1962. Physicochemical hydrodynamics. Prentice Hall.

Lucas, D., Krepper, E., Prasser, H. M., 2007. Use of models for lift, wall and turbulent dispersion forces acting on bubbles for poly-disperse flows. Chemical Engineering Science 62, 4146–4157.

Lucas, D., Tomiyama, A., 2011. On the role of the lateral lift force in poly-dispersed bubbly flows. International Journal of Multiphase Flow 37, 1178–1190.

Lucas, D., Ziegenhein, T., 2019. Influence of the bubble size distribution on the bubble column flow regime. International Journal of Multiphase Flow 120, 103092.

Magnaudet, J., Mougin, G., 2007. Wake instability of a fixed spheroidal bubble. Journal of Fluid Mechanics 572, 311–337.

Mei, R., Klausner, J., Lawrence, C., 1994. A note on the history force on a spherical bubble at finite Reynolds number. Physics of Fluids 6, 418–420.

Moore, D. W., 1965. The velocity of rise of distorted gas bubbles in a liquid of small viscosity. Journal of Fluid Mechanics 23, 749–766.

Naciri, A., 1992. Contribution à l'étude des forces exercées par un liquide sur une bulle de gaz: portance, masse ajoutée et interactions hydrodynamiques. Ph.D. thesis, Ec. Centrale Lyon, France.

Rastello, M., Marie, J. L., Lance, M., 2011. Drag and lift forces on clean spherical and ellipsoidal bubbles

in a solid-body rotating flow. Journal of Fluid Mechanics 682, 434–459.

Rybczynski, W., 1911. On the translatory of a fluid sphere in a viscous medium. Bulletin of the Academy of Sciences, Kracow, Series A, 40–46.

Schiller, V. L., Nauman, A. Z., 1933. Uber die grundlegenden berechnungen bei der schwerkraftaufbereitung. Zeitschridt Vereines Deutscher Ingenieure 77, 318–320.

Tomiyama, A., 1998. Struggle with computational bubble dynamics. Multiphase Science and Technology 10, 369–405.

Tomiyama, A., 2004. Drag, lift and virtual mass forces acting on a single bubble. In: the 3rd International Symposium on Two-Phase Flow Modelling and Experimentation. Pisa, Italy.

Tomiyama, A., Kataoka, I., Zun, I., Sakaguchi, T., 1998. Drag coefficients of single bubbles under normal and micro gravity conditions. JSME International Journal Ser. B: Fluids and Thermal Engineering 41(2), 472–479.

Tomiyama, A., Tamai, H., Žun, I., Hosokawa, S., 2002. Transverse migration of single bubbles in simple shear flows. Chemical Engineering Science 57, 1849–1858.

Tomiyama, A., Žun, I., Sou, A., Sakaguchi, T., 1993. Numerical analysis of bubble motion with the VOF method. Nuclear Engineering and Design 141, 69–82.

Tsuge, H., Hibino, S., 1977. The onset conditions of oscillatory motion of single gas bubbles rising in various liquids. Journal of Chemical Engineering of Japan 10, 66–68.

Žun, I., 1980. The transverse migration of bubbles influenced by walls in vertical bubbly flow. International Journal of Multiphase Flow 6, 583–588.

Ziegenhein, T., Tomiyama, A., Lucas, D., 2018. A new measuring concept to determine the lift force for distorted bubbles in low Morton number system: Results for air/water. International Journal of Multiphase Flow 108, 11–24.